

Nanoscale Abrasive Wear of CoCrMo in In Situ TEM Sliding

Yifeng Liao · Emily Hoffman · Laurence D. Marks

Received: 5 August 2014 / Accepted: 19 November 2014
© Springer Science+Business Media New York 2015

Abstract The mechanical behaviour of materials at nanometre dimensions has been a major recent topic of research. In this study, the wear properties of a ~ 60 -nm thin foil made of the ductile fcc phase of a CoCrMo alloy were examined using in situ sliding test in a transmission electron microscope by sliding a silicon AFM tip on the fcc matrix under an applied normal load of 416–1,279 nN. The material near the surface was deformed plastically, forming dislocations and dislocation cells at the surface. The wear process was found to be strongly dependent on extrinsic factors, namely the attack angle between the tip and the CoCrMo surface. At an attack angle of 64° , the surface was removed by continuous fractures 40–73 nm below the surface. At a lower attack angle of 24° , the abrasive wear switched to ploughing.

Keywords Nanotribology · Cobalt · In situ · TEM

1 Introduction

Wear is a progressive material degradation near the surface under sliding contact. Wear models at the macroscopic level based on continuum theories have been well documented, both experimentally and theoretically, with great success in predicting wear behaviour [1–4]. In their seminal work, Tabor and Bowden [5–8] suggested that the

interface encompasses a large number of micro- or nanoscale single asperities. Despite the successful macroscopic models [9–11], wear behaviour of a single small asperity is still largely unclear, especially when the asperity scale decreases to tens of nanometres [12]. There has been a reasonable amount of interest in nanoscale sliding, most of the research involving wearless experiments [13–18]. Experimental results of deformation caused by a single asperity sliding are very limited. Of note are in situ wear studies in a scanning electron microscope (SEM) by Bates et al. and Kato et al. which revealed substantial details on ploughing, wedging, and cutting of a wide variety of materials [19–22]. However, the feature size of these SEM experiments was $\sim 1 \mu\text{m}$. Precisely how the material is deformed *at* and *beneath* the surface remains a mystery.

With the recent development of precise sample manipulation in a transmission electron microscope (TEM), directly observing wear at the nanoscale has become accessible through in situ TEM sliding tests. This technique has provided unprecedented information of materials evolution during sliding. A number of phenomena were discovered, such as sliding-induced recrystallization [23], liquid-like behaviour [13, 24], and thermally activated wear recently reported by Jacobs and Carpick under non-load conditions [16], in which the Archard law does not fully account for the wear processes. These new behaviours, not commonly observed at the macroscopic scale [25], call into question the validity of classical models such as abrasive wear as applied to nanoscale single sliding asperities. This is a concern for structural materials with excellent plasticity that are able to accommodate large deformation.

In this work, we present an in situ TEM study of abrasive wear of a CoCrMo fcc phase, which is ductile in its bulk form [26, 27], sliding against a silicon atomic force

Electronic supplementary material The online version of this article (doi:10.1007/s11249-015-0471-z) contains supplementary material, which is available to authorized users.

Y. Liao (✉) · E. Hoffman · L. D. Marks
Department of Materials Science and Engineering, Northwestern
University, Evanston, IL 60208, USA
e-mail: Yifeng.Liao@gmail.com

microscope (AFM) tip. CoCrMo alloy is a well-known wear-resistant material that has broad applications ranging from gas turbines to medical implants. This alloy consists of ductile fcc phase and brittle carbides [28–30]. Due to the small size of the TEM–AFM tip, we were able to selectively test the fcc region to quantify the behaviour of the ductile phase.

2 Experimental

An as-cast CoCrMo alloy complying with the ASTM standard F75 for metal hip replacement was cut into a foil of $20\ \mu\text{m} \times 5\ \mu\text{m} \times \sim 60\ \text{nm}$ thickness using a FEI Helios dual-beam focused ion beam. The two sides were $\sim 1.5\ \mu\text{m}$ thick and fixed to the TEM grid. The foil was initially cut at 30 kV and finished with 2 kV cleaning. The CoCrMo thin foil was then slid against a silicon AFM tip in situ in a 200 kV F20 Tecnai TEM in vacuum. The AFM tip, which was provided by Nanofactory, was fabricated by using SF₆ plasma isotropic etching, followed by oxidation and sharpening. The AFM–TEM apparatus has been described in details elsewhere [31]. The normal load was applied along the z -axis and can be calculated by the deflection of the cantilever (x): $F = kx$, with the spring constant k of the cantilever being $\sim 5.2\ \text{N/m}$. The normal load in the sliding test was 416–1,279 nN, equivalent to 144–230 MPa. The lateral force measurement is not available with this AFM–TEM sliding apparatus. The dynamical event was recorded using a TV camera. The videos were analysed frame by frame. Static images with higher resolution were obtained using a CCD camera.

Finite element analysis was performed using a simplified model to estimate the stress state at the contact area. A normal pressure of 200 MPa was applied to the centre region (100 nm wide) of the top edge of a $20\ \mu\text{m} \times 5\ \mu\text{m} \times 60\ \text{nm}$ lamella. The two sides of the lamella were set to be fixed to match that the two sides of the FIB foil were thick and welded to the TEM grid. A total number of 189,756 nodes were used for the analysis.

3 Results

The silicon tip showed no discernible wear, similar to the sliding test on a carbide phase reported elsewhere [31]. The specimen exhibited substantial abrasive wear. Figure 1a–c shows TEM images of a region before and after the sliding test. A number of strips s with a nearly uniform spacing of $\sim 70\ \text{nm}$ were present prior to the sliding test. The strips are straight and parallel to each other, indicating they resided on certain crystallographic planes. These are stacking faults commonly seen in CoCrMo alloys due to

the low stacking fault energy [32, 33]. The sliding involved substantial plastic deformation in the subsurface. Figure 1d shows the surface region before and after one sliding pass. The bend contours arrowed with dark arrows were unchanged indicating that sample bending due to sliding was negligible. Since the diffraction conditions for the two images are similar, the darker contrast in the region enclosed in the white lines after the sliding test must be associated with plastic deformation. Dislocations were generated during compression/sliding and appeared to be impeded by the stacking faults, forming localized dislocation cells as highlighted by the white lines. For completeness, we note that the fact that stacking faults can act as barriers to dislocation motion is well established.

Volume loss occurred via chipping when the thin foil slides towards the right-hand side as shown in Fig. 2 and Supplemental Video 1. The applied pressure was 144–230 MPa. The area indicated with an arrow in Fig. 2b was removed during the first sliding pass. A curved, 236-nm-long crack was formed, with the maximum depth of 40 nm beneath the surface. In $<0.03\ \text{s}$, the crack propagated through the sample and a chip, volume $\sim 3.7 \times 10^5\ \text{nm}^3$, fractured away from the surface. A second crack, 382 nm long with a maximum depth of 73 nm, was formed in the subsequent sliding, resulting in a volume loss of $\sim 1.2 \times 10^6\ \text{nm}^3$. The geometry of the crack is highlighted with the dotted line in Fig. 2. One end of the crack was at the surface behind the AFM tip, while the other end was closed ahead of the tip in the subsurface. There are no other newly formed defects (e.g. dislocations, stacking faults or cracks) near the fresh surface. The attack angle, α , which is the angle between the sample surface and the counter surface, was 64° , as shown in Fig. 2c.

Ploughing occurred when the thin foil slid towards the left-hand side in the area close to where the chipping took place, see Fig. 3 and Supplemental Video 2. The normal load was 416–1,024 nN. Due to the larger contact area because of wedge formation, the pressure was calculated to be 25–61 MPa. We note that this was a fresh area which the tip did not slide on previously. A small volume was dug out and accumulated ahead of the tip. The ploughing was continuous with no abrupt cracking. The attack angle was 24° , as shown in Fig. 3. The silicon asperity penetrated the surface to a depth of $\sim 52\ \text{nm}$. The ploughing process occurred over 2 s and 1,160 nm with the ploughed volume moving together with the sliding tip. The pile-up volume after ploughing was $\sim 3.0 \times 10^6\ \text{nm}^3$.

4 Discussion

Materials at the nanoscale may exhibit different plasticity behaviour than the bulk. Higher strength and mechanical annealing are observed in nanoindentation of micropillars

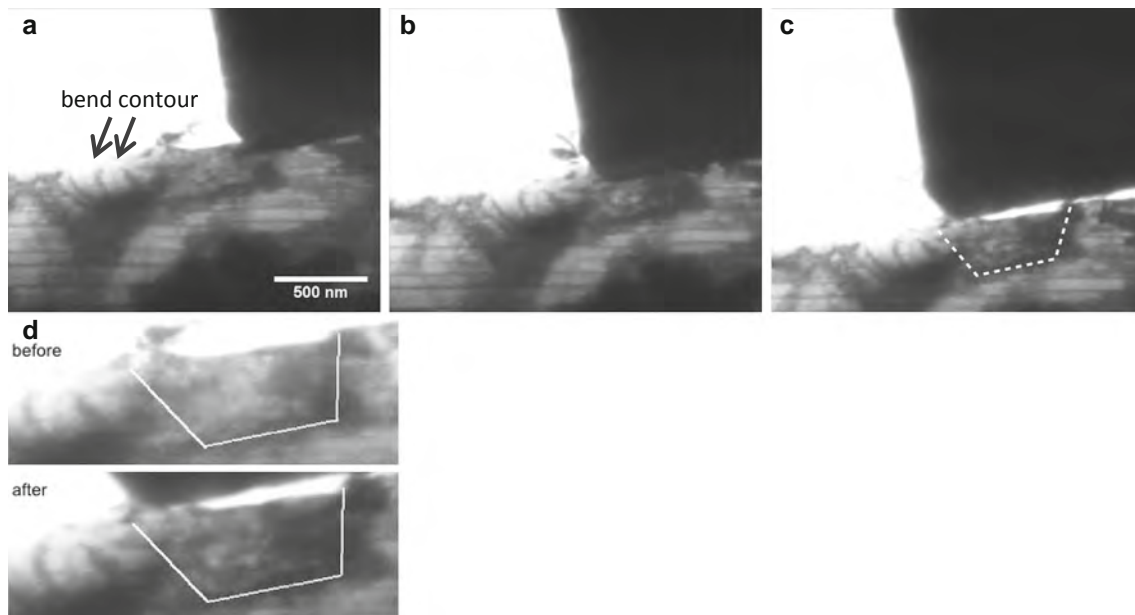


Fig. 1 a–c Series of TEM micrographs showing plastic deformation in the CoCrMo fcc phase. A dislocation cell is highlighted with the dotted lines. The bend contour arrowed in (a) changed minimally,

indicating that the sliding contact did not bend the thin foil. d The contact region before and after sliding, showing the deformation with dark contrast

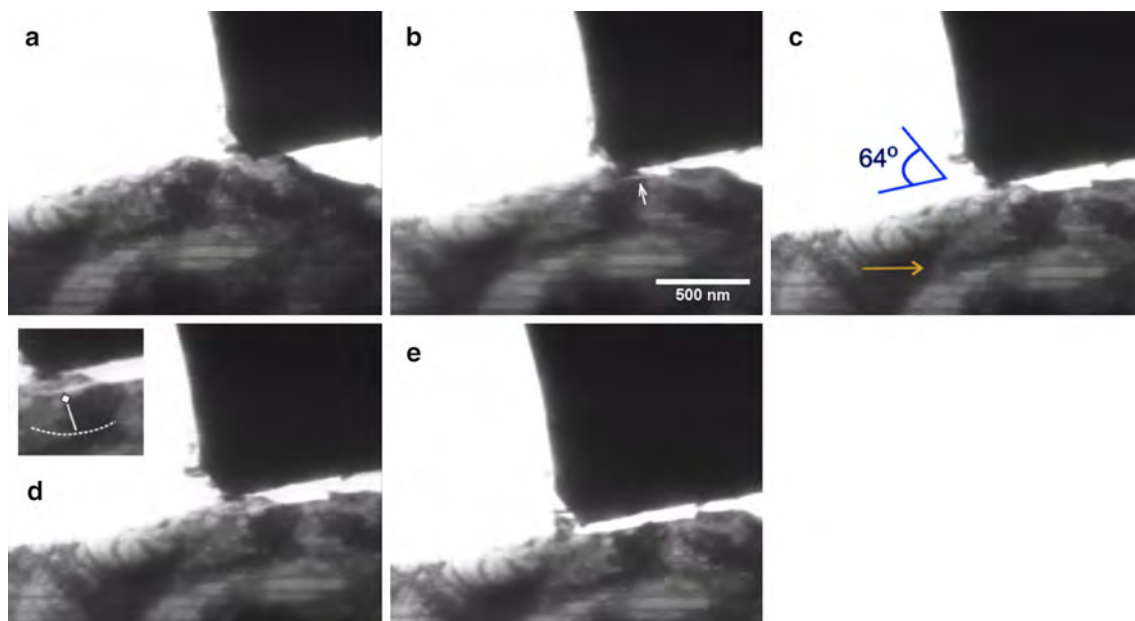


Fig. 2 Series of TEM micrographs showing chipping of the CoCrMo fcc phase. The attack angle is 64° . A crack is highlighted in the inset figure in (d)

[34–37], as the flow process is influenced by the limited number of dislocation sources. In order to elucidate the stress state of the in situ sliding of the CoCrMo thin foil, a simplified model where a 60-nm-thick lamella is loaded by a constant applied pressure of 200 MPa from the top edge was analysed using finite element analysis (Abaqus software). It is worth noting that despite the thin nature of the

FIB foil as a whole, the thickness of the lamella is comparable to the contact interface. Thus, one should not consider that the contact area is in a plain stress state. As shown in Fig. 4, the maximum shear stress in the lamella is ~ 190 MPa at the surface and gradually decreases in the subsurface region. Similarly, the maximum von Mises stress is ~ 165 MPa at the surface.

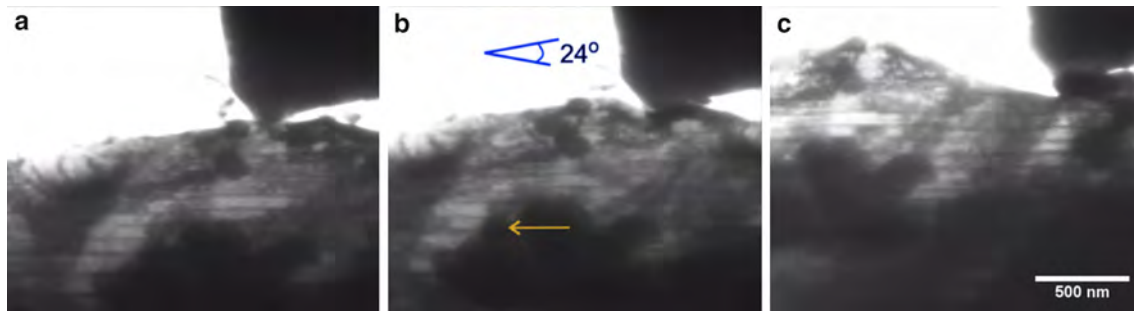


Fig. 3 Series of TEM micrographs showing wear via ploughing. The CoCrMo thin foil was moving towards the *left*. **a** The initial stage. **b** The tip grooved into the fcc phase. The attack angle is $\sim 24^\circ$. **c** Ploughing lasted for 1,160-nm sliding distance, forming an edge ahead of the tip

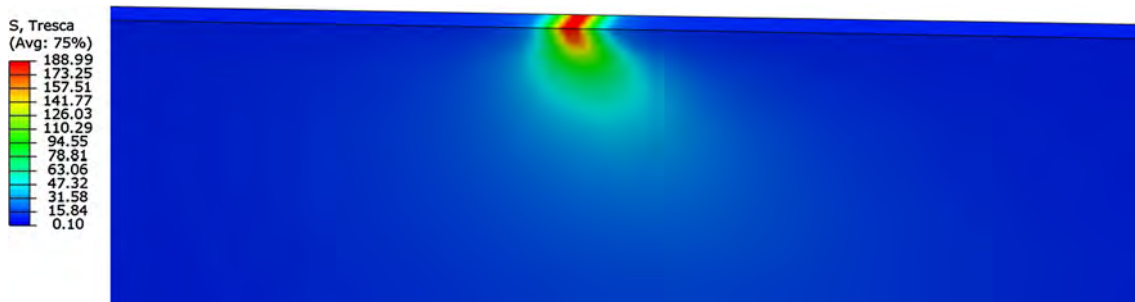


Fig. 4 Finite element analysis of a simplified thin lamella with a constant applied pressure of 200 MPa on the centre of the top surface. The two sides were fixed. The maximum shear stress is decreased below the contact surface

Although both the Tresca stress and von Mises stress are much less than the yield strength of bulk CoCrMo, the surface exhibited significant plastic deformation, evident in the dislocation cells. The sliding-induced localized deformation at the surface may be the origin of a layer of nanocrystalline material, extensively reported in the post facto TEM examinations of metallic materials after conventional wear tests with repeated sliding [12, 38–40]. Sliding did not anneal the existing defects, in this case stacking faults. This is consistent with the previous observations of plastic deformation in sliding contact tests at multiple length scale. In the recent molecular dynamic (MD) simulation by Mishra and Szlufarska, wear was found to be controlled by substantial dislocation activities in the subsurface, within a few nanometres of the contact interface. Zhao and Bhushan also observed bend contours and dislocations in a TEM thin foil deformed *ex situ* at a load of 80 μN using an AFM tip and concluded that plastic flow is primarily responsible for volume removal [41].

Wear is known to be a multifactorial phenomenon dependent on not only the materials properties, but also the contact geometry. The attack angle is critically important to how material is removed. At the lower angle of 24° , the active wear mechanism was ploughing; wear switched to abrupt chipping at the attack angle of 64° . This finding agrees with the experimental observations of abrasive wear

in situ in a SEM reported by Kato and co-workers [20, 22], in which ploughing is favoured at an attack angle of 0° – 40° , while cutting is favoured at $>40^\circ$. Our result suggests that the continuum models are largely valid at the nanometre scale.

In the ploughing, the volume removed from the surface was deformed plastically and junction growth is favourable, presumably due to the small angle between the surface and the tip. The ploughing came to an end when the plastically deformed junction was large enough to support the applied load as shown in Fig. 3. As suggested by Hokkirigawa and Kato, ploughing leads to a higher resistance to friction [21]. The geometry dependence of the transition from cutting to ploughing at ~ 1 nm scale is also reported in the MD simulation of Mishra and Szlufarska [42]. Thus, wear is sensitive to the contact profile across the length scale from the atomistic to micrometre scale.

The chipping featured nanoscale cracking. The crack in Fig. 2 might initiate at the surface behind the sliding tip or in the subsurface and be closed in the subsurface ahead of the tip due to the compressive stress. The crack shape is in accordance with the trajectory of the maximum shear stress as extensively described in slip line theory [43]. Thus, the cracking seems to be dominated by mode II shear crack, in agreement with the analysis by Hearle and Johnson [44]. No vertical cracks were generated during the sliding,

indicating that vent crack theory [45, 46] for brittle materials does not account for the surface fracture. Similarly, the surface delamination theory [47], which has been considered as not responsible for the wear involving plasticity, does not account for the wear process, because the crack was generated by the shear stress.

While the classic models are still largely valid in this abrasive wear at the nanometre scale, there are differences. Shear cracks are usually attributed to the plastic deformation created by cyclic sliding. The cracks were formed in the first sliding pass. Single sliding can generate large surface deformation; thus, cyclic sliding is unnecessary. This could be due to existing defects, or the reduced mechanical properties at the surface, known as a salvage layer. Surface oxide in this in situ sliding test is complicated. The surface oxide layer formed prior to the in situ TEM sliding tests can lower the adhesion as described in Ref. [3, 48]. Once the surface oxide was removed by sliding, the oxidation of the metal freshly exposed is significantly slower than in a one atmospheric due to the low vacuum in a TEM, typically better than 10^{-7} torr. The electron beam also leads to strong desorption and reduction of any oxides or chemisorbed oxygen at the metal surface, further suppressing the oxidation. Thus, we believe that surface oxide does not play a major role in these experiments after the initial stage when the surface oxide is removed.

5 Conclusions

In situ sliding of CoCrMo fcc matrix has revealed the details of abrasive wear at the nanometre scale. The continuum models are still largely valid for a single sliding asperity of 100 nm. The surface was deformed plastically. The wear process is critically dependent on the attack angle. Under similar sliding conditions, a lower angle of 24° led to ploughing. A junction was formed in front of the tip during ploughing. A higher attack angle of 64° led to chipping. The curved surface fracture was induced by the shear stress via mode II fracture.

Acknowledgments This work was funded by the NSF under the Grant Number CMMI-1030703. The Electron Microscopy Center of Argonne National Laboratory is acknowledged for the use of their facilities. Ms. Gwendolyn Reid is acknowledged for proof reading the manuscript.

References

- Dowson, D.: History of tribology. Professional Engineering Publishers, London (1998)
- Johnson, K.L.: Contact mechanics. Cambridge University Press, Cambridge (1985)
- Hutchings, I.M.: Tribology: friction and wear of engineering materials. Edward Arnold, London (1992)
- Williams, J.A.: Engineering tribology. Oxford University Press, Oxford (1994)
- Bowden, F.P., Tabor, D., Gane, N., Willis, R.F.: Solid surfaces under static and sliding contact—some recent work on microdeformation and chemical reactivity. *Z. Phys. Chem-Leipzig* **244**, 129 (1970)
- Gane, N., Bowden, F.P.: Microdeformation of solids. *J. Appl. Phys.* **39**, 1432 (1968)
- Bowden, F.P., Tabor, D.: The friction and lubrication of solids. Clarendon Press, Oxford (1950)
- Bowden, F.P., Moore, A.J.W., Tabor, D.: The ploughing and adhesion of sliding metals. *J. Appl. Phys.* **80**, 80–91 (1942)
- Bhushan, B.: Contact mechanics of rough surfaces in tribology: multiple asperity contact. *Tribol. Lett.* **4**, 1–35 (1998). doi:[10.1023/A:1019186601445](https://doi.org/10.1023/A:1019186601445)
- Bhushan, B.: Handbook of micro/nanotribology. CRC Press, Boca Raton (1995)
- Bhushan, B., Majumdar, A.: Fractal theory of the interfacial temperature distribution in the slow sliding regime. 1. Elastic contact and heat-transfer analysis—discussion. *J. Tribol. T. ASME* **116**, 822 (1994). doi:[10.1115/1.2927339](https://doi.org/10.1115/1.2927339)
- Rigney, D.A.: Comments on the sliding of wear of metals. *Tribol. Int.* **30**, 361–367 (1997)
- Marks, L.D., Warren, O.L., Minor, A.M., Merkle, A.P.: Tribology in full view. *MRS Bull.* **33**, 1168–1173 (2008)
- Gotsmann, B., Lantz, M. A.: Atomistic wear in a single asperity sliding contact. *Phys. Rev. Lett.* **101**, 125501 (2008)
- Bhaskaran, H., et al.: Ultralow nanoscale wear through atom-by-atom attrition in silicon-containing diamond-like carbon. *Nat. Nanotechnol.* **5**, 181–185 (2010)
- Jacobs, T.D.B., Carpick, R.W.: Nanoscale wear as a stress-assisted chemical reaction. *Nat. Nanotechnol.* **8**, 108–112 (2013)
- Gnecco, E., Bennewitz, R., Meyer, E.: Abrasive wear on the atomic scale. *Phys. Rev. Lett.* **88**, 215501 (2002)
- Szlufarska, I., Chandross, M., Carpick, R.W.: Recent advances in single-asperity nanotribology. *J. Phys. D Appl. Phys.* **41**, 123001–123039 (2008)
- Bates, T.R., Ludema, K.C., Brainard, W.A.: Rheological mechanism of penetrative wear. *Wear* **30**, 365–375 (1974). doi:[10.1016/0043-1648\(74\)90150-1](https://doi.org/10.1016/0043-1648(74)90150-1)
- Kato, K.: Micromechanisms of wear—wear modes. *Wear* **153**, 277–295 (1992). doi:[10.1016/0043-1648\(92\)90274-C](https://doi.org/10.1016/0043-1648(92)90274-C)
- Hokkirigawa, K., Kato, K.: An experimental and theoretical investigation of plowing, cutting and wedge formation during abrasive wear. *Tribol. Int.* **21**, 51–57 (1988). doi:[10.1016/0301-679x\(88\)90128-4](https://doi.org/10.1016/0301-679x(88)90128-4)
- Kato, K., Kayaba, T., Endo, Y., Hokkirigawa, K.: Three dimensional shape effect on abrasive wear. *J. Tribol.* **108**, 346–349 (1986)
- Liao, Y., EswaraMoorthy, S.K., Marks, L.D.: Direct observation of tribological recrystallization. *Phil. Mag. Lett.* **90**, 219–223 (2010). doi:[10.1080/09500830903571384](https://doi.org/10.1080/09500830903571384)
- Merkle, A.P., Marks, L.D.: Liquid-like tribology of gold studied by in situ TEM. *Wear* **265**, 1864–1869 (2008). doi:[10.1016/j.wear.2008.04.032](https://doi.org/10.1016/j.wear.2008.04.032)
- Luan, B.Q., Robbins, M.O.: The breakdown of continuum models for mechanical contacts. *Nature* **435**, 929–932 (2005). doi:[10.1038/Nature03700](https://doi.org/10.1038/Nature03700)
- Jacobs, J.J., et al.: Metal-on-metal bearing surfaces. *J. Am. Acad. Orthop. Sur.* **17**, 69–76 (2009)
- Liao, Y., et al.: New insights into hard phases of CoCrMo metal-on-metal hip replacements. *J. Mech. Behav. Biomed.* **12**, 39–49 (2012)

28. Stemmer, P. et al.: Microstructure of retrievals made from standard cast HC-CoCrMo alloys. ASTM-STP, (2012, in print)
29. Pourzal, R., et al.: Subsurface changes of a MoM hip implant below different contact zones. *J. Mech. Behav. Biomed.* **2**, 186–191 (2009). doi:[10.1016/j.jmbbm.2008.08.002](https://doi.org/10.1016/j.jmbbm.2008.08.002)
30. Clemow, A.J.T., Daniell, B.L.: Solution treatment behavior of Co-Cr-Mo alloy. *J. Biomed. Mater. Res.* **13**, 265–279 (1979)
31. Liao, Y., Marks, L. D.: Direct observation of layer-by-layer wear. (2014, submitted)
32. Dillamor, I.L.: The stacking fault energy dependence of the mechanisms of deformation in fcc metals. *Metall. Trans.* **1**, 2463–2470 (1970)
33. Rajan, K., Vandersande, J.B.: Room-temperature strengthening mechanisms in a Co-Cr-Mo-C alloy. *J. Mater. Sci.* **17**, 769–778 (1982). doi:[10.1007/Bf00540374](https://doi.org/10.1007/Bf00540374)
34. Uchic, M.D., Dimiduk, D.M., Florando, J.N., Nix, W.D.: Sample dimensions influence strength and crystal plasticity. *Science* **305**, 986–989 (2004)
35. Chisholm, C., et al.: Dislocation starvation and exhaustion hardening in Mo alloy nanofibers. *Acta Mater.* **60**, 2258–2264 (2012). doi:[10.1016/j.actamat.2011.12.027](https://doi.org/10.1016/j.actamat.2011.12.027)
36. Shan, Z.W., Mishra, R.K., Asif, S.A.S., Warren, O.L., Minor, A.M.: Mechanical annealing and source-limited deformation in submicrometre-diameter Ni crystals. *Nat. Mater.* **7**, 115–119 (2007)
37. Minor, A.M., et al.: A new view of the onset of plasticity during the nanoindentation of aluminium. *Nat. Mater.* **5**, 697–702 (2006). doi:[10.1038/Nmat1714](https://doi.org/10.1038/Nmat1714)
38. Buscher, R., et al.: Subsurface microstructure of metal-on-metal hip joints and its relationship to wear particle generation. *J. Biomed. Mater. Res. B* **72B**, 206–214 (2005). doi:[10.1002/Jbm.B.30132](https://doi.org/10.1002/Jbm.B.30132)
39. Buscher, R., Fischer, A.: The pathways of dynamic recrystallization in all-metal hip joints. *Wear* **259**, 887–897 (2005). doi:[10.1016/j.wear.2005.02.036](https://doi.org/10.1016/j.wear.2005.02.036)
40. Bryant, M., et al.: Characterisation of the surface topography, tomography and chemistry of fretting corrosion product found on retrieved polished femoral stems. *J. Mech. Behav. Biomed.* **32**, 321–334 (2014)
41. Zhao, X.Z., Bhushan, B.: Material removal mechanisms of single-crystal silicon on nanoscale and at ultralow loads. *Wear* **223**, 66–78 (1998). doi:[10.1016/S0043-1648\(98\)00302-0](https://doi.org/10.1016/S0043-1648(98)00302-0)
42. Mishra, M., Szlufarska, I.: Dislocation controlled wear in single crystal silicon carbide. *J. Mater. Sci.* **48**, 1593–1603 (2013). doi:[10.1007/s10853-012-6916-y](https://doi.org/10.1007/s10853-012-6916-y)
43. Challen, J.M., Oxley, P.L.B.: Explanation of the different regimes of friction and wear using asperity deformation models. *Wear* **53**, 229–243 (1979). doi:[10.1016/0043-1648\(79\)90080-2](https://doi.org/10.1016/0043-1648(79)90080-2)
44. Hearle, A.D., Johnson, K.L.: Mode-II stress intensity factors for a crack parallel to the surface of an elastic half-space subjected to a moving point load. *J. Mech. Phys. Solids* **33**, 61 (1985). doi:[10.1016/0022-5096\(85\)90022-5](https://doi.org/10.1016/0022-5096(85)90022-5)
45. Lawn, B.R., Swain, M.V.: Microfracture beneath point indentations in brittle solids. *J. Mater. Sci.* **10**, 113–122 (1975). doi:[10.1007/Bf00541038](https://doi.org/10.1007/Bf00541038)
46. Lawn, B.R., Fuller, E.R.: Equilibrium penny-like cracks in indentation fracture. *J. Mater. Sci.* **10**, 2016–2024 (1975). doi:[10.1007/Bf00557479](https://doi.org/10.1007/Bf00557479)
47. Suh, N.P.: Delamination theory of wear. *Wear* **25**, 111–124 (1973)
48. Varenberg, M.: Towards a unified classification of wear. *Friction* **1**, 333–340 (2013)